Cool Stars, Stellar Systems and the Sun
ASP Conference Series, Vol. 154, 1998
eds. R. A. Donahue and J. A. Bookbinder

DEM Reconstruction: A Markov-Chain Monte-Carlo Approach

Vinay Kashyap and Jeremy Drake

Smithsonian Astophysical Observatory, 60 Garden St., Cambridge, MA 02138

Abstract:

We describe a Markov-Chain Monte-Carlo process using a Metropolis algorithm to derive Differential Emission Measures (DEMs) and element abundances from EUV line fluxes. This technique allows us to relax the smoothness constraint generally imposed on DEMs and also to determine confidence bounds on the computed values. We apply this method to solar spectral line data from SERTS (Solar EUV Rocket Telescope and Spectrograph).

1. Introduction

The Differential Emission Measure (DEM) distribution is a convenient way to characterize the temperature structure of Solar and stellar coronae, and is observationally derived from measurements of spectral emission (see e.g., Craig & Brown 1976, Bruner & McWhirter 1988). The intensity of an optically thin spectral line arising from a transition ($u \to l$) in a collision-dominated plasma is

$$I_{ul} = A\ K_{ul} \int G_{ul}(T) N_e^2(T)\ dV(T)\,, \tag{1}$$

where A is the abundance of the element producing the spectral line, K_{ul} is a known constant that includes the energy of the transition and distance factors, and $G_{ul}(T)$ is the "contribution" function of the line at a temperature T incorporating all the relevant atomic physics data and ion balance calculations. Recasting this integral into one over T,

$$I_{ul} = A\ K_{ul} \int_{\Delta T} G_{ul}(T) \mathrm{DEM}(T)\ d\log T \quad , \tag{2}$$

where $\mathrm{DEM}(T) = N_e^2(T) \frac{dV(T)}{d\log T}$ is the DEM in its logarithmic differential form.

Thus the DEM may be inferred from a given a set of observed line fluxes and associated contribution functions, either by inverting the above integral equation (e.g., Harrison & Thompson 1991 and references therein; Schmitt et al. 1996; Judge, Hubeny, & Brown 1997) or via a forward-fitting process (e.g., Stern et al. 1995; Monsignori-Fossi & Landini 1991; Brosius et al. 1996). The structure of the DEM is consequently dependent on which spectral lines are detectable in the observed energy range and the temperature sensitivity of these lines. Hence it is not determinable at temperatures which are not traced by any specified line.

2. Algorithm

The algorithm is described in detail and applied to test cases by Kashyap & Drake (1997a,b). Here we give a brief overview of the basis of the algorithm.

Bayes' Theorem allows us to determine the probability distribution of model parameters used to describe the observed data. The (joint) probability of a specified set of n model parameters $M = \{M_\nu, \nu = 1..n\}$ given the set of m data points $D = \{D_i, i = 1..m\}$,

$$p(M|D) = p(M)\frac{\prod_{i=1,m} p(D_i|M)}{p(D)} \tag{3}$$

(see e.g., Loredo 1990), where $p(M)$ is the *a priori* joint probability of the model parameters (which are assumed to be independent of each other), $p(D_i|M)$ is the likelihood of observing the the given datum D_i for the specified set of model parameters, and $p(D)$ is a normalization factor. Determination of $p(M|D)$ constitutes a complete solution to the problem of model parameter estimation.

A **Markov Chain** is an ordered sequence of random variables $X_0, X_1, X_2, ...$, such that the probability distribution of X_{i+1} is dependent directly only on X_i. Each X_i here represents a particular realization of the model parameters: The Markov-Chain may be completely specified by giving the *a priori* distributions for the initial state X_0 and transition rules for going from state X_i to X_{i+1}. Such a process is appropriate as a searching scheme to find the (usually small) volume in the (usually large) parameter space where the model describes the data well (e.g., where $\int p(\{M_i\}|D)dM_1..dM_\nu > 0.9$).

When the number of parameters are large, and/or $p(M|D)$ is complicated, it may not be possible to characterize the distribution analytically, but rather a sample of points must be drawn from it and the distribution characterized in an approximate sense. In particular, we can obtain estimates of the marginalized distribution for each parameter by driving a Markov Chain with a *Monte Carlo* sampling process. A Monte-Carlo Markov-Chain (**MCMC**) will converge to a persistent distribution[1] (i.e., sampling from $p(M|D)$) regardless of the initial state as the number of trials increase if the defined Markov-Chain is

invariant (a persistent distribution of parameters *exists* for the given problem),

homogeneous (the transition rules do not change with time), and

ergodic (any valid set of model parameters may be obtained with non-zero probability from any other valid set).

The **Metropolis** algorithm (Metropolis et al. 1953) defines a possible set of transition rules to determine a new set of parameters (M') from an existing set (M):

[1] The convergence is stochastic, in the sense that regardless of how large the number of trials n may be, after a sufficiently large number of trials $m >> n$, X_m will be nearly independent of X_n, though still close to the persistent distribution.

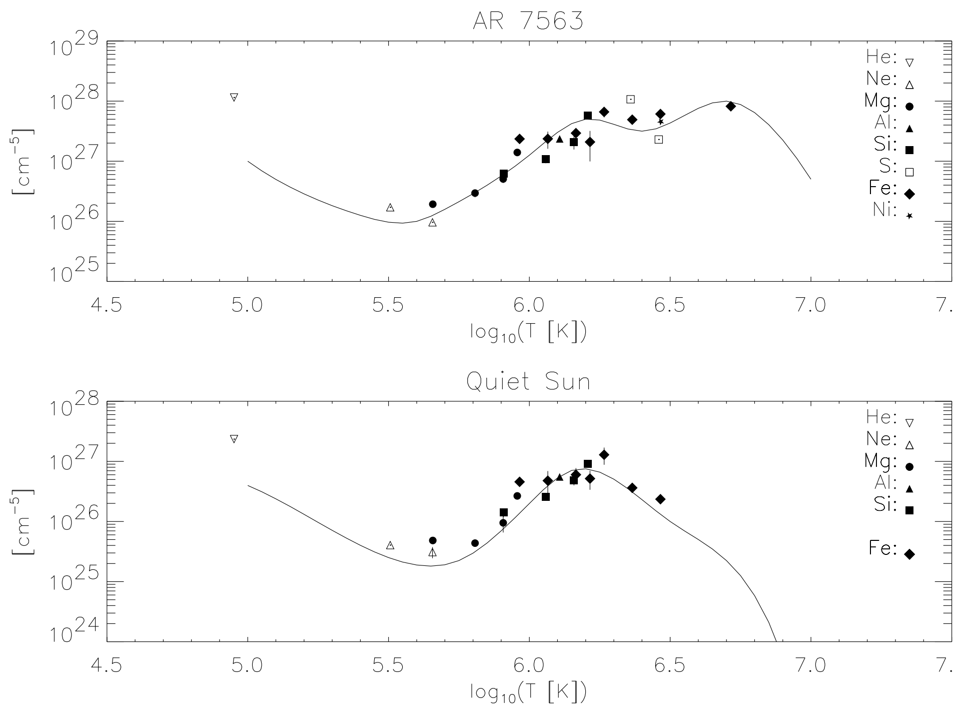

Figure 1. Emission Measures (EM) [cm^{-5}] derived from combining all lines for particular ions, for the Active (upper panel) and Quiet Sun (lower panel) regions observed by SERTS. Error bars have been shown when multiple lines from the same ion have been combined to produce a single ion-averaged EM. Each symbol refers to an ion of a particular element, as listed to the right. Following Brosius et al. (1996), we have assumed solar coronal abundances derived by Feldman et al. (1992). The DEMs [cm^{-5}] derived by Brosius et al. are represented by the solid curves. Note the scatter in the EMs predicted by individual lines. A simple DEM curve without an estimate of its uncertainty is clearly inadequate.

Select a candidate set M^* in which all components except for a subset $\{k\}$ are the same as in M, while the subset of parameters are chosen at random from a *proposal distribution* given by the probabilities $S_k(M, M^*)$.

Accept the candidate set with probability $A(M, M^*)$; else **reject** it and retain the old set. A popular choice for $A(M, M^*)$ is simply the ratio of the likelihoods, $A(M, M^*) = min(1, \frac{P(D|M^*)}{P(D|M)})$.

3. SERTS Data

A solar active region (NOAA AR7563) and quiet sun regions were observed during a flight of the Solar EUV Rocket Telescope and Spectrograph (SERTS)

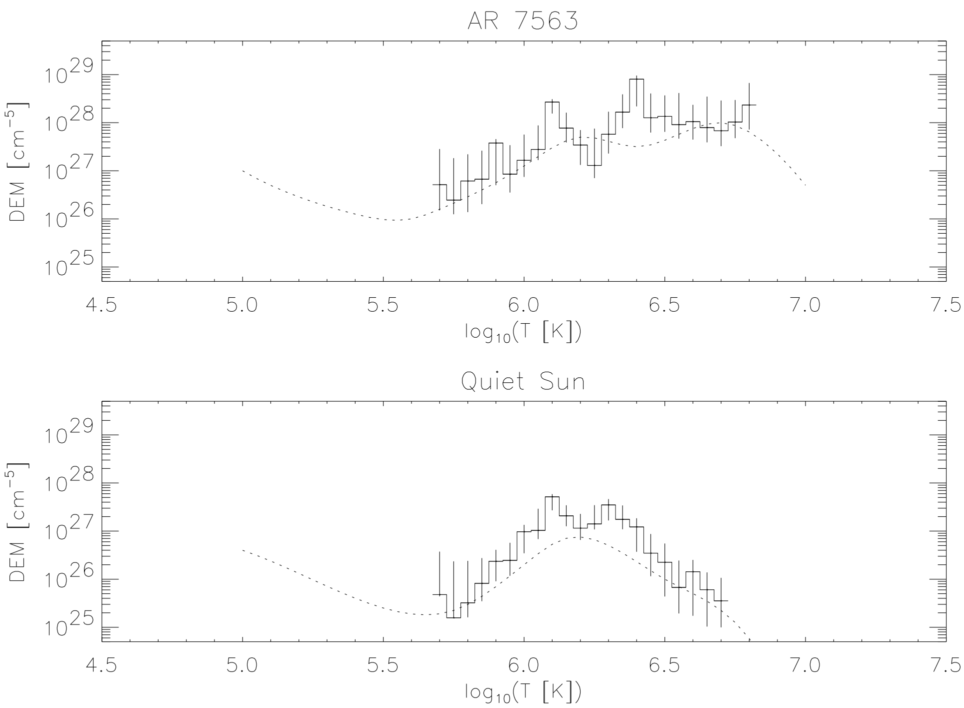

Figure 2. Active (upper panel) and Quiet Sun (lower panel) region DEMs (stepped line) derived with the MCMC[M] technique, assuming solar photospheric abundances measured by Grevesse et al. (1992), involving 500 simulations/point, and using the same lines as used by Brosius et al. (1996) (dataset [A]). Electron densities of 5×10^9 and 10^9 cm^{-3} were assumed for the Active and Quiet Sun regions respectively. Where line information is absent, the DEM is not well-determined and is not shown here. The dotted lines show the DEMs derived by Brosius et al. (1996). The width of the steps indicate the width of the temperature bins and the vertical bars denote 95% confidence limits on the derived $DEM(T)$.

in the 280 – 420 Å region (17 Aug 1993; cf., Brosius et al. 1996). Subsequent analysis by Brosius et al. resulted in the detection and identification of 65 lines in the active region spectrum and 57 lines in the quiet region spectrum. Brosius et al. obtain cubic spline fits of DEMs to a subset of the data – spectral lines whose line ratios are temperature and density insensitive. These DEMs are shown in Figure 1, along with the Emission Measures (EM) derived for individual line fluxes and averaged over all lines for given ions. The large scatter in the EMs predicted by individual lines clearly show that a simple DEM curve without an estimate of its uncertainty is clearly inadequate.

We apply the MCMC(M) algorithm outlined above to the spectral lines in the SERTS database to reconstruct the DEM. The implementation of the algorithm for the case of DEMs derived from spectral line fluxes (and associated errors) is described in detail by Kashyap & Drake (1997a,b). Briefly, we model

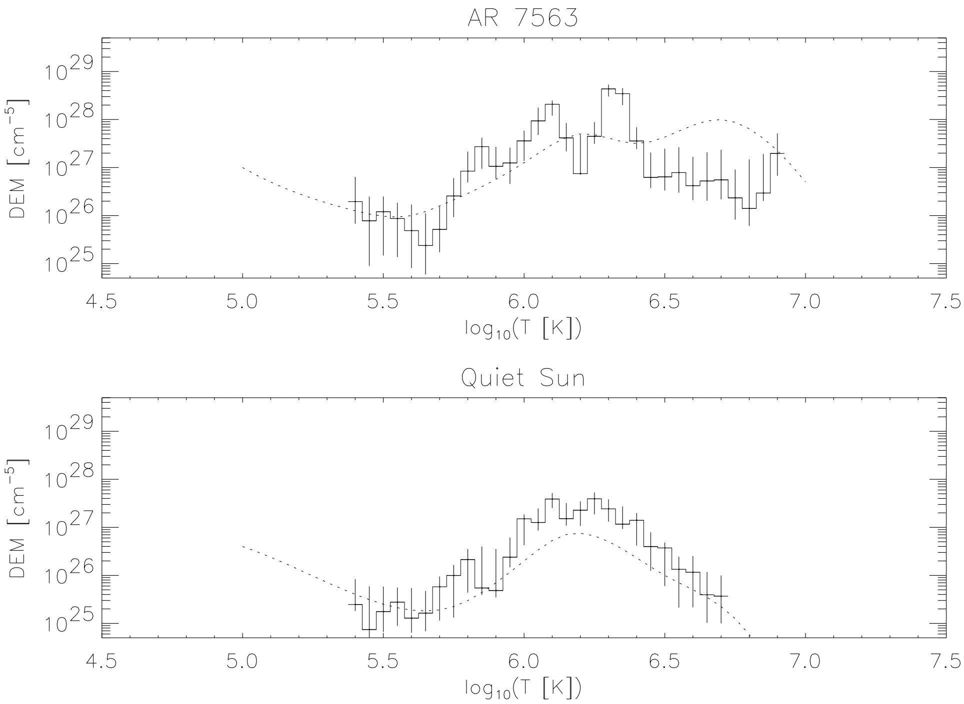

Figure 3. As in Figure 2, but derived from the full SERTS line list (dataset [B]).

the DEM as a set of independent parameters at various temperatures which are smoothed locally at a scale defined by the width of the contribution functions $G_{ul}(T)$ (we thus eliminate the "global" smoothing present in spline curve fits). We compute model line fluxes for the parametrized DEM and abundances, using updated ion balance calculations (Arnaud & Rothenflug 1986; Arnaud & Raymond 1992) and atomic data compiled in the CHIANTI database (Dere et al. 1997).

4. Results

We reconstruct DEMs for different sets of the available line list:

A: The set of lines whose flux ratios are density- and temperature-insensitive; this is the same lines as used by Brosius et al. (1996) (Figure 2).

B: The full set of lines available with the exception of He II λ304 (Figure 4).

C: A subset of the available lines chosen to minimize systematic errors (cf. Kashyap & Drake 1997b) (Figure 3).

The DEMs derived using the MCMC[M] technique are clearly different from the DEMs constructed by Brosius et al., and we attribute the source of the differences to our use of updated atomic data (CHIANTI; Dere et al. 1997), improved

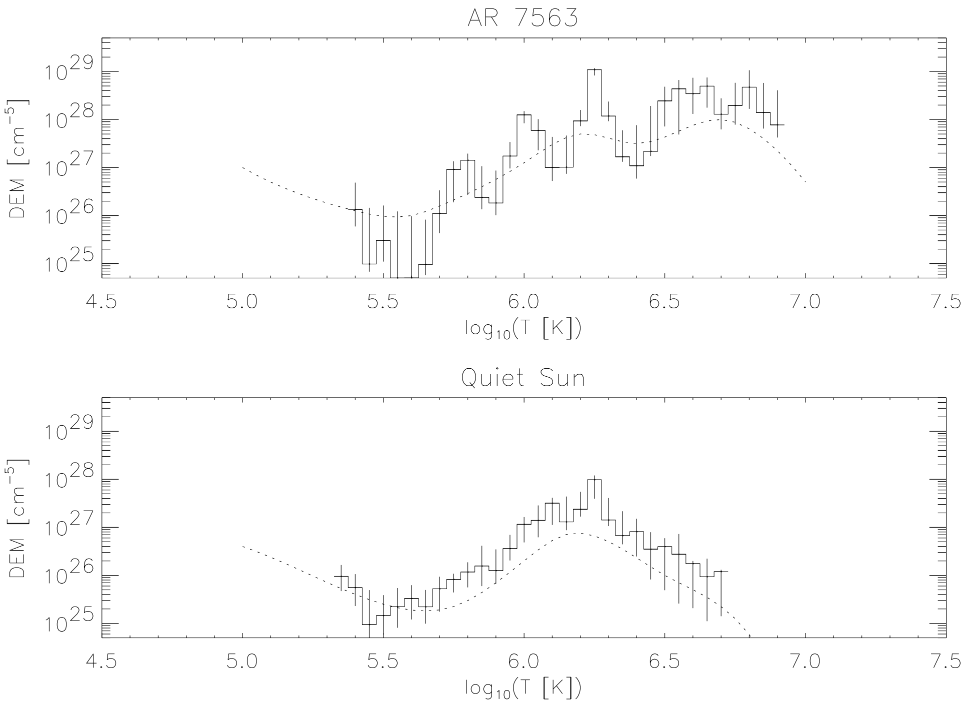

Figure 4. As in Figure 2, but derived from a line list designed to minimize systematic errors (dataset [C]).

ion balance calculations (Arnaud & Rothenflug 1986; Arnaud & Raymond 1992), avoidance of global smoothing constraints, and also to differences in adopted abundances (we use solar photospheric abundances derived by Grevesse et al. 1992; the lower photospheric abundances of low-FIP elements result in higher estimates of DEM(T), which is reflected in the figures). The reconstructed DEMs also show that the shape and structure of the DEM is strongly dependent on the chosen line list and the quality of the available atomic data. Note, for example, the large drop in the DEM at $\log T > 6.5$ in dataset [B] which is caused by the inclusion of S XIV λ417.6 (see Kashyap & Drake 1997b).

The quality of the reconstruction may be judged by Figure 5, which compares the predicted and observed fluxes for dataset [B]. The temperature coverage of the lines included in the dataset is also illustrated. The effect of varying the abundances is also shown.

Acknowledgments. We thank Peter Freeman for useful comments. VK was supported by NASA grants during the course of this research. JD was supported by the *AXAF* Science Center NASA contract NAS8–39073.

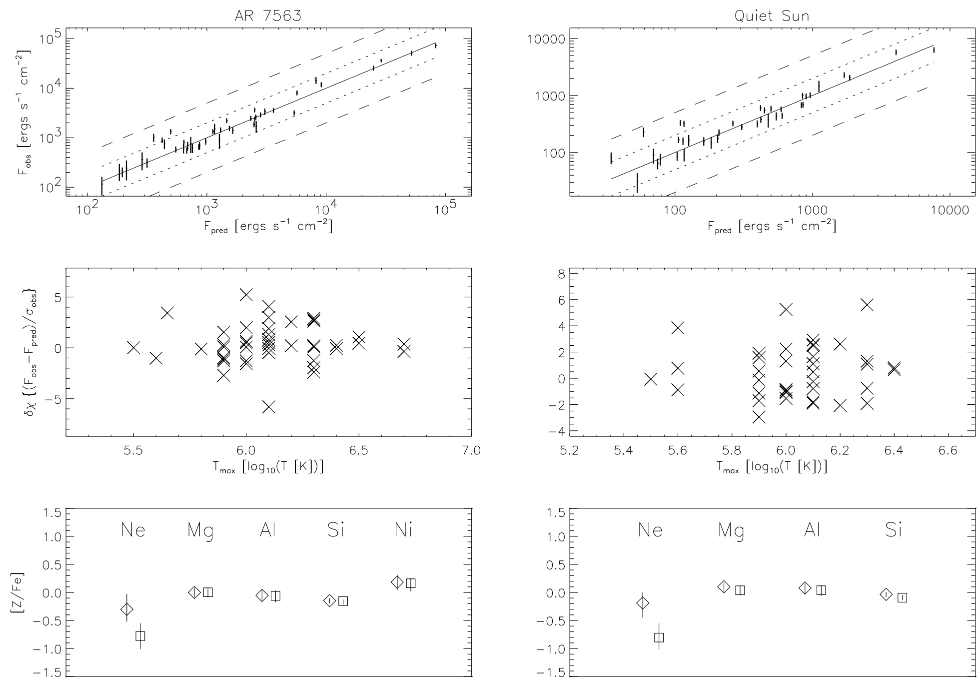

Figure 5. Quality of the DEM Reconstruction, for data set [C]: The plots on the left describe the Active Region DEM, while those on the right describe the Quiet Sun DEM. The upper panels compare the observed and predicted fluxes: the solid line represents $F_{\rm observed} = F_{\rm predicted}$, the dotted and dashed lines represent factors of 2 and 5 departures from equality respectively; the solid vertical lines show the 2σ error bars on the observed fluxes. The middle panels show the temperature coverage of the lines and the quality of the fit to each line: the scatter at a given temperature must be ascribed to uncertainties in the atomic data. The lower panels show the results of allowing abundances to vary relative to Fe. The diamonds and squares represent baseline Fe abundances from Grevesse et al. (1992; photospheric) and Feldman et al. (1992; coronal) respectively; the solid vertical lines indicate 95% error bars on the estimates.

References

Arnaud, M., & Raymond, J.C. 1992, ApJ, 398, 394

Arnaud, M., & Rothenflug, R. 1986, A&AS, 60, 425

Brosius, J.W., Davila, J.M., Thomas, R.J., & Monsignori-Fossi, B.C. 1996, ApJS, 106, 143

Bruner, M.E., & McWhirter, R.W.P. 1988, ApJ, 326, 1002

Craig, I.J.D., & Brown, J.C. 1976, A&A, 49, 239

Dere, K.P., Landi, E., Mason, H.E., Monsignori-Fossi, B.C., & Young, P.R. 1997, A&AS, in press

Feldman, U., Mandelbaum, P., Seely, J.F., Doschek, G.A., & Gursky, H. 1992, ApJS, 81, 387

Grevesse, N., Noels, A., & Sauval, A.J. 1992, in Proc. 1^{st} SOHO Workshop, Coronal Streamers, Coronal Loops and Coronal and Solar Wind Composition, ESA SP–348, ESA Publ. Div., ESTEC, Noordwijk, 305

Harrison, R.A., & Thompson, A.M. 1991, Intensity Integral Inversion Techniques: a Study in Preparation for the SOHO Mission, SERC Technical Report RAL–91–092

Judge, P.G., Hubeny, V., & Brown, J.C. 1997, ApJ, 475, 275

Kashyap, V., & Drake, J.J. 1997a, in High Resolution Solar Atmospherics Dynamics Workshop, eds. L. Golub, J.A. Bookbinder, & E.E. DeLuca (San Francisco: ASP), in press

Kashyap, V., & Drake, J.J. 1997b, ApJ, in preparation

Loredo, T.J. 1990, in Maximum Entropy and Bayesian Methods, ed. P.F. Fougere (Dordrecht: Kluwer), 81

Metropolis, N., Rosenbluth, A.W., Rosenbluth, M.N., Teller, A.H., & Teller, E. 1953, J.Chem.Phys., 21, 1087

Monsignori-Fossi, B.C., & Landini, M. 1991, SERC Technical Report RAL-91-092, eds. R.A. Harrison & A.M. Thompson, 27

Neal, R.M. 1993, Technical Report CRG-TR-93-1, Dept. of Computer Science, University of Toronto

Schmitt, J.H.M.M., Drake, J.J., Stern, R.A., & Haisch, B. 1996, ApJ, 457, 882

Stern, R.A., Lemen, J.R., Schmitt, J.H.M.M., & Pye, J.P. 1995, ApJ, 444, L45